Stony Brook University

OFFICIAL COPY

The official electronic file of this thesis or dissertation is maintained by the University Libraries on behalf of The Graduate School at Stony Brook University.

© All Rights Reserved by Author.

Study of bulk and surface currents

limiting the performance of GaSb -based semiconductor devices

A Thesis Presented

by

Muralidhar Kumar

to

The Graduate School

in Partial Fulfillment of the

Requirements

for the Degree of

Master of Science

in

Electrical Engineering

Stony Brook University

May 2008

Stony Brook University

The Graduate School

Muralidhar Kumar

We the thesis committee for the above candidate for the

Master of Science degree, hereby recommend

acceptance of this thesis.

Dmitri Donetski-Thesis Advisor

Assistant Professor, Department of Electrical & Computer Engineering

Ridha Kamoua-Chairperson of Defense

Associate Professor, Department of Electrical & Computer Engineering

Vladislav. A. Kuzminskiy

Research Scientist, Department of Electrical & Computer Engineering

Vladimir Zaitsev

Director of Labs-CME, Department of Materials Science and Engineering.

This thesis is accepted by the Graduate School

Lawrence Martin

Dean of the graduate school

Abstract of the Thesis

Study of bulk and surface currents

limiting the performance of GaSb-based semiconductor devices

by

Muralidhar Kumar

Master of Science

in

Electrical Engineering

Stony Brook University

2008

Bulk and surface currents limiting the performance of GaSb based semiconductor devices were studied. In thermophovoltaic applications recombination currents limit the open circuit voltage. The first section of this work dealt with the study of carrier recombination in InGaAsSb epitaxial layers for thermophotovoltaic applications. Minority carrier lifetimes of p-type InGaAsSb lattice matched to GaSb were studied using Time Resolved Photoluminescence. The temperature dependence of lifetimes of the samples differed from the expected $T^{1.5}$ model and this variation was explained by the absorption tail below band gap and the temperature dependence of photon recycling. The values of radiative recombination coefficient B and Auger coefficient C were calculated. Radiative and non radiative lifetimes were separated and radiative efficiency was found to be 67 %.

The second section of the work dealt with the reduction of surface currents by passivation of GaSb based Schottky diodes using micromachining and pulsed anodization technique. Surface currents in untreated Schottky diodes fabricated by photolithography and micromachining were compared. It was found that micromachining does not damage the surface and that devices fabricated by micromachining had lower surface currents when compared to devices fabricated from conventional processing. Passivation by pulsed anodization resulted in the reduction of the surface current by 10-11times.

Table of Contents

List of figures vii

List of Tables x

Section 1- Carrier Recombination in 0.52 eV p-type InGaAsSb

Lattice Matched to GaSb

1. Introduction 1
2. Experiment 2
3. Results and Discussion 3

Determination of Shockley-Read-Hall and Auger Coefficients

4. Experiment 7
5. Theoretical Analysis and Results 9
6. Conclusion 11
7. References 12

Section 2 - Surface Passivation of GaSb-based Semiconductor Devices

1. Introduction 28
2. Fabrication and characterization of Ti-GaSb based Schottky contact 30
3. Results and discussion 32

4. Conclusion 34

5. References 35

List of Figures

Figure 1.1: Experimental set up used in TRPL technique. 14

Figure 1.2: Temperature dependence of carrier lifetime of InGaAsSb DH's. Solid dots are experimental points of sample with doping 4×10^{17}; the straight line is a theoretical fit. 15

Figure 1.3: Temperature dependence of Integrated PL intensity. Inset shows emission spectra at various temperatures. 16

Figure 1.4: Transmission spectrum of 04-959.The dashed line represents the transparency point T/T_0. It is observed that T/T_0 can not be determined accurately. 17

Figure 1.5: Absorption spectrum of heavily doped sample 04-969 (broken line) along with its experimental spontaneous emission spectrum. For energy range till 0.52 eV the experimental PL spectrum was converted to absorption and matched to the experimental spectrum. This is shown as a solid line. 18

Figure 1.6: Absorption spectrum of moderately doped 04-959(solid line) and its experimental spontaneous emission spectrum. Square root fit given by the expression: $\frac{A\sqrt{h\nu - E_g}}{h\nu}$ is shown as a broken line. 19

Figure 1.7: Experimental absorption spectrum of 04-959(A), 04-969(B) and the calculated spectrum obtained after by BM factor(C). Rapid increase of absorption is seen above 0.65 eV and is attributed to absorption from GaSb substrate. The Luminescence is negligible after this point and does not affect calculation of Photon Recycling. 20

Figure 1.8: PR coefficient obtained from experimental absorption spectrum (points) and from multiplying corresponding BM factors to the absorption spectrum of 04-959(curve). 21

Figure 1.9: Temperature dependence of Photon Recycling for sample doped 4×10^{17}. Photon recycling varies as $T^{0.54.}$ 22

Figure1.10: Calculated Temperature dependence of Radiative lifetimes of InGaAsSb for various doping concentrations. Temperature dependence of Photon recycling is taken into account. 23

Figure1.11: Integrated PL intensity as a function of Excess carriers at low excitation. The undoped sample was excited using a 650 nm, 20 mW CW laser in order to achieve low level of excess carrier concentration. Super linear behavior confirms Shockley Read Hall recombination. 24

Figure1.12: Gaussian Profile of the Nd: YAG Laser. The full width half maximum of the profile is taken to be the diameter of the spot. 25

Figure1.13: Radiative efficiency as a function of excess carriers with C as a parameter. Values of A and B were obtained from experimental lifetimes 26

Figure1.14: Experimental PL per excess carrier concentration of undoped sample, shown as solid points are compared to the simulated radiative efficiency for various values of C. The sample was excited with a 532 nm Q switched Nd: YAG laser with pulse 0.5 ns pulse width and repetition rate of 7 KHz.. 27

Figure 2.1: Schematic of the micromachining apparatus 36

Figure 2.2: Dependence of the groove depth on average laser power. Inset shows the cross section of the sample obtained by micromachining with radius R and depth D.The top contact is a Schottky contact while the bottom contact is ohmic. 37

Figure 2.3: Steps in obtaining the Schottky contact with surface passivation by a native oxide 38

Figure 2.4: I-V characteristics of Schottky diode with mesa radius 236 μm with Ti contact showing the rectifying properties of the barrier 39

Figure 2.5: I-V characteristics of Schottky diodes with metal contact radii of 65,120, and 225 μm from bottom to top, respectively. 40

Figure 2.6: Dependence of the saturation current per mesa circumference versus the mesa radius for samples micromachined at different average power levels P. 41

Figure 2.7: The device saturation current per mesa circumference versus the device radius. The circles and squares represent Schottky diodes with no passivation and with oxide passivation. The offsets (which are the surface current densities) were determined to be (1.18 ± 0.16) nA/μm and (0.11 ±0.07) nA/μm, respectively. 42

List of Tables:

Table 1: Surface currents obtained for various micromachining power levels and the errors in calculating them 43

Carrier Recombination in 0.52 eV p-type InGaAsSb Lattice Matched to GaSb

Introduction

InGaAsSb photovoltaic cells with band gap 0.5-0.6 eV are essential for high conversion efficiency in Thermophotovoltaic (TPV) systems having thermal sources at temperatures near 1000°C [1]. InGaAsSb materials lattice matched to GaSb have band gap around 0.5 eV. They offer flexibility in band structure engineering [2] while reducing defects and resulting in good carrier lifetime [3-4]. There is interest in developing both fabrication techniques [5-7] and device design [8] of InGaAsSb based TPV cells. Phototransistors and Avalanche photodiodes based on InGaAsSb are also being developed [9-10]. Study of recombination phenomena in InGaAsSb then assumes importance because reducing carrier recombination results in high performance of TPV cells [11-12]. A better understanding of the mechanisms behind carrier recombination will help to further improve device performance. This work focuses on explaining the temperature dependence of minority carrier lifetimes and predicts the behavior of lifetimes at various temperatures and doping concentrations.

Experiment

Temperature dependences of minority carrier lifetime in zinc doped (p-type) InGaAsSb double heterostructures (DH) were determined using Time Resolved Photoluminescence (TRPL) technique. The set of DH's were grown on GaSb substrates with active layer thickness of 2μm and various doping concentrations. A schematic of the set up used to determine lifetime is shown in Figure 1.1. The InGaAsSb sample was excited by means of a 532 nm Q switched Nd: YAG laser with pulse width 0.5 ns and repetition rate of 7 KHz. Reflective optics were used to focus the beam on the sample. The emitted radiation was collected using objective lenses and focused onto an InSb broad band photo detector. The signal from the detector was amplified and fed to a digital scope with a data acquisition rate of 5 Gs/s. The Photoluminescence (PL) decays were averaged; an exponential decay over two orders of magnitude then gave an accurate value of the measured lifetime. A cryostat was used to vary the temperature range of the sample.

Results and discussion

Figure 1.2 shows the lifetimes of an InGaAsSb DH with doping 4×10^{17} obtained at various temperatures. The squares are experimental points. The slope of inverse lifetimes is less than the expected $T^{1.5}$ dependence and is given by T^{β} with β=1.26. The theoretical fit obtained by taking into account temperature dependence of photon recycling and reduced density of states is shown as a straight line.

The Integrated PL intensity was also obtained using the same setup as in Figure 1.1, except that the photo detector was connected to a Stanford Research Systems SR 810 DSP Lock-in Amplifier. Integrated PL intensity is a proportional to the total number of carriers that recombine radiatively. The current in the photo detector, fed directly to the Lock-in is then a measure of the integrated PL intensity. The intensities obtained as a function of temperature are shown in Figure 1.3. At 77 K it is assumed that all carriers recombine radiatively. It is observed that the integrated PL intensity is fairly constant from 77 K to 200 K implying that the recombination is almost completely radiative. Non radiative recombination begins to contribute after 200 K, reducing the number of carriers that combine radiatively and thus the current in the lock- in amplifier decreases.

Absorption Edge Measurements

Absorption curve of the sample is necessary to determine photon recycling. A Thermo Nicolet Fourier Transform Infrared Spectrometer (FTIR) Nexus 670 was used to observe the transmission spectrum of the samples and absorption is obtained by Lambert's law $T = T_0e^{-\alpha x}$ where T/T_0 gives the fraction of intensity of light transmitted and α is the absorption. The mean value of the sinusoidal curve shown in Figure 1.4 was taken as the value of T/T_0, but as seen from the figure; its accurate determination was not possible. Small changes in T/T_0, affected the absorption tails significantly but not absorption at higher energies. To calculate absorption tails accurately, the experimental PL spectrum was converted to absorption spectrum and scaled to match the experimental absorption for energies 0.52 eV and below (shown in Figure 1.5). The absorption spectra of two of the samples, a heavily doped (sample number 04-969, doping = 3×10^{18} cm^{-3})

and a moderately doped (sample number 04-959, doping = 2.55×10^{17} cm^{-3}) are shown in Figures 1.5 and 1.6 respectively. The absorption edge spectrum can be approximated by the square root function ($\alpha_{squareroot}$)

$$\alpha_{squareroot} = \frac{A\sqrt{h\nu - E_g}}{h\nu} \quad (1)$$

where hν is photon energy in eV, E_g is band gap of the sample. This square root dependence is also shown in Figure 1.6 for 04-959.One can see that it fits the experimental absorption spectrum for lower energy ranges.

The experimental absorption curve was split into 3 intervals and fitted with polynomials for numerical integration. A 2nd order polynomial was used for energy range (0.51-0.54 eV) and a 5th order polynomial was used for energy range (0.54-0.62 eV). The polynomials fit the experimental curves almost exactly and are hardly seen in the figure till 0.62 eV. The square root approximation described above was used for higher energy ranges (0.62-0.78 eV) where absorption due to GaSb substrate increased noise significantly.

A distinct drop in the absorption for the same photon energies of the highly doped sample can be seen in Figure 1.7. This drop is attributed to Burstein Moss (BM) effect which occurs in heavily doped materials where most of the states near band edges are occupied by carriers, increasing the optical band gap.

The BM factor is given by [14]

$$BM = 1 - \left(\frac{1}{1 + \exp\left\{ \frac{\varepsilon(\nu) - F_h}{K_b T} \right\}} \right) \quad (2)$$

where $\varepsilon(\nu) = \Delta\varepsilon \cdot m_{cv}/m_v$ and $\Delta\varepsilon = (h\nu - E_g)$, m_{cv} is the reduced effective mass given by $(m_c \cdot m_v)/(m_c+m_v)$ and F_h is the quasi Fermi level for holes. m_c and m_v, the relative masses of electrons and holes and were found to be 0.0385 m_e and 0.3863 m_e respectively. Figure 1.7 shows the absorption spectrum of the moderately doped sample (curve A), the absorption spectrum of highly doped 04-969 (curve B) and the calculated absorption spectrum obtained when the absorption spectrum of the moderately doped sample (where band filling effects are negligible) is multiplied by the BM factor (curve C) . There is a

close match between the two spectra confirming Burstein Moss effect. At higher energy ranges, the calculated spectrum deviated from the actual absorption and this was attributed to change in effective electron mass.

Photon recycling

Photon Recycling is the increase in carrier lifetime due to self absorption of radiation in materials. The radiation emitted by recombination of electrons and holes has energy larger than the band gap energy and is reabsorbed to create more electron hole pairs. This effect causes an increase in radiative lifetime and is characterized by the Photon recycling (PR) coefficient. PR varies with thickness of the active region and the number of times light is reflected inside the active region before it escapes. The PR of a number of the samples with different doping concentrations (p-type) was calculated by calculating the overlap between absorption and spontaneous emission, as described in [13] by taking into account multiple reflections from the surface. The coefficients obtained from experimental absorption curves are shown as solid squares in Figure 1.8. The absorption spectrum of sample 04-959 (doping 2.55×10^{17} $cm^{-}3$) was multiplied by BM factors corresponding to different doping concentrations as given by (2) and using these absorption spectra PR coefficients were obtained. The PR coefficients so obtained are shown as a curve in Figure 1.8. The PR coefficient of sample 04-959 is 3.58, which is lower than the commonly accepted value of 4 for InGaAs materials[15]. It is observed that photon recycling coefficient decreases with increase in doping. The spontaneous emission spectrum shrinks towards lower energy ranges as temperature decreases and thus the PR decreases. Photon Recycling was found to vary as $T^{0.54}$ as shown on Figure 1.9.

Minority Carrier Lifetime

Spontaneous emission rate (Q) is the rate of decay of excess carriers $\Delta p/\tau$ and the minority carrier lifetime is given by:

$$\tau = - \Delta p / Q \quad (3)$$

$$Q = \frac{8\pi N^2}{h^2 c^3} \int_{0.514}^{0.78} \frac{\alpha(h\nu)\cdot(h\nu^2)}{\left[\exp\left[\frac{(h\nu - e_g)m_{cv}/m_c - F_e}{k_b T}\right]+1\right]\left[\exp\left[\frac{(h\nu - e_g)m_{cv}/m_v - F_h}{k_b T}\right]+1\right]} \qquad (4)$$

The theoretical approach is given in [13].

τ was determined to be 16 ns at 300K for a doping of 4×10^{17} cm^{-3}. In calculating Fermi levels of majority carriers Nilsson's global approximation has been used[16].

$$\frac{1}{\tau} = B\times\Delta p \qquad (5)$$

where B is the Radiative recombination coefficient. The lifetimes so obtained had to be multiplied by their Photon recycling coefficients to obtain true radiative lifetime,

$$\tau_r = \tau\times PR \qquad (6)$$

Value of B thus obtained was 1.5×10^{-10} cm^3/s at 300 K. A theoretical fit to the experimental lifetimes shown in Figure 1.1 was made by simulating the radiative lifetimes using (6). Since lifetimes are completely radiative till 200 K, lifetimes calculated by (6) were almost equal to the experimental lifetimes in this temperature range. Absorption tails indicated the presence of states below band gap. The effective band gap was taken to be 0.52 eV and the effective density of states were taken to be 0.8 of Nc and Nv. Using these two parameters (band gap and density of states) the radiative lifetimes were modeled over a wide range of temperature(20 K- 300 K). A close fit to experimental lifetimes in the temperature range 30 K- 200 K is observed. Above 200 K, non radiative effects tend to affect the lifetimes since the integrated PL intensity dropped at temperatures above 200 K. The difference in lifetime between experimental points and the simulated radiative lifetime is then attributed to non radiative recombination. Non radiative lifetime thus obtained was 133 ns at 300K and the radiative efficiency was found to be 67%.

The radiative lifetimes (τ_r) of different doping concentrations were simulated and are shown in Figure 1.10. Estimation of actual radiative lifetime requires the temperature dependence of both Photon recycling coefficient and of τ.

Determination of Shockley-Read -Hall and Auger Coefficients

Experiment

In order to study the contributions of Shockley Read Hall (SRH) and Auger recombination to the non radiative lifetime an undoped sample (3 μm thick) was used. To examine the presence of SRH recombination, the undoped sample was excited using a 650 nm, 20 mW CW laser in order to achieve low levels of excess carrier concentration (around 10^{16}-10^{17} cm^{-3}). Integrated PL intensity was obtained as a function of excitation power by connecting the photo detector to a Stanford Research Systems SR 810 DSP Lock-in Amplifier and the integrated PL intensity was determined in the same manner as described in section 1.3. Figure 1.11 shows the Integrated PL as a function of excitation power for the sample with thickness 3 μm at 300 K. The experimental curve was super linear at very low excitations. This implied presence of SRH recombination and indicated a range of excess carrier concentration that began to saturate the defect centers and hence radiative recombination increased super linearly with excitation. Once all defect centers saturate, radiative recombination is predominant. At room temperature the non radiative lifetime of the sample doped $4\times10^{17}cm^{-3}$ was taken to be due to Shockley-Read-Hall (SRH) recombination as excess carrier concentration was not high enough to be dominated by Auger process. The inverse of this lifetime gave the Shockley-Read-Hall recombination coefficient A which has a value $8.33\times10^{-6}\,s^{-1}$.

To study Auger recombination, a very high excess carrier concentration was required. The sample was excited with a 532 nm Q switched Nd: YAG laser with 0.5 ns pulse width and repetition rate of 7 KHz. Reflective optics were used to focus the beam on the sample. In order to get higher concentration of excess carriers a focusing lens was used. The emitted radiation was collected using objective lenses and focused onto a photo detector. Beam profile measurements were carried out to determine the size of the spot in order to determine instantaneous excess carrier concentration. A HP 8153A Lightwave multimeter was placed on the spot where the sample was excited and a blade was used to slowly uncover the beam using a motorized travel stage along the vertical

and horizontal axis. The gradual change in intensity detected by the silicon head of the light wave meter was differentiated to get a Gaussian curve as shown in Figure1.12. The full width half maximum (FHWM) of the curve was taken to be the diameter of the spot.

Theoretical Analysis and Results

The theoretical analysis for interpreting the experimental integrated PL intensity is given below.

The decay of excess carriers can be expressed by

$$\frac{dn}{dt} = -\left(A\Delta n + B(p+\Delta n)\Delta n + C(p+\Delta n)^2\Delta n\right)$$

$$\int_{\Delta n}^{0} \frac{d\Delta n}{A\Delta n+B(p+\Delta n)\Delta n+C(p+\Delta n)^2\Delta n} = -\int_{0}^{t} dt \quad (7)$$

The Integrated PL intensity per excess carrier concentration is equivalent to the radiative efficiency and can be expressed as

$$\frac{I}{\Delta n} = \int_{\Delta n}^{0} \frac{B\Delta n^2(t)dt}{\Delta n}$$

From (7),

$$\frac{I}{\Delta n} = -\int_{\Delta n}^{0} B\frac{d\Delta n}{A+B(p+\Delta n)+C(p+\Delta n)^2} \quad (8)$$

A,B,C are the Shockley Read Hall , radiative recombination and Auger coefficients, Δn is the concentration of excess carriers, p the background doping and I the Integrated PL Intensity.

With values of A, B known the right hand side of expression (8) was evaluated numerically, by assuming a value for C, and changing the limits of integration i.e. the excess carrier concentration. The process was repeated for a number of different values of C to obtain a family of curves as shown in Figure 1.13 with doping p assumed to be 4×10^{17}. Figure 1.14 shows the same family of simulated curves and compares it to experimental points. The excitation pulse was very short when compared to the lifetimes

of carriers and the repetition rate was low enough to ensure that all carriers recombined before the onset of next pulse. The instantaneous excess carrier density was then determined accurately because the excitation power, the area and period of excitation were known. Comparing the experimental points to the theoretical curves at high excess carrier concentrations, C was estimated to be to be 5×10^{-29} cm^6/s .This is lower than the value obtained by Kumar et.al[17] who report a value of 1×10^{-28} cm^6/s. The experimental curve is super linear at very low excitations where SRH recombination is present. Once all defect centers saturate, recombination is predominantly radiative. At very high excess concentrations Auger process begins to dominate. Thus radiative efficiency reaches a maximum and then decreases when Auger recombination controls the minority carrier lifetime. The low value of C implies that the sample is not Auger limited and hence can be doped to a level of 1×10^{18}, beyond which Auger recombination reduces the radiative efficiency. Photon recycling coefficient decreases with doping as seen from Figure 1.8 and this effect can be offset by including a back surface reflector to confine radiation within the active region and increase recycling.

Conclusion:

Deviation of radiative recombination from $T^{1.5}$ dependence was observed experimentally in 0.52 eV InGaAsSb epitaxial materials grown lattice matched to GaSb. This behavior was explained with the effect of density of states below band gap and photon recycling. Photon recycling coefficient was calculated by taking into account multiple reflections. The radiative recombination coefficient B was calculated to be 1.5×10^{-10} cm^3/s at 300 K. Good agreement of the model was observed with experimental lifetimes in wide temperature range 30-200 K. Radiative and non radiative lifetimes were separated and Auger coefficient C was estimated to be 3- 5×10^{-29} cm^6/s at 300 K. This value is lower than previously predicted. The low value of C allows increased doping in TPV devices up to the level of 1×10^{18} which can lead to higher open circuit voltage. The decrease of recycling with higher doping can be overcome by including a back surface reflector.

References

[1] M.W. Dashiell et al *IEEE. T. Electron. Dev.* 53**,** 2879 (2006).

[2] C.A.Wang *Indium Phosphide and Related Materials Conf. IPRM. 14th (Stockholm)* pp. 709-12 (2002).

[3] C.A. Wang, H.K.Choi, G.W. Turner, D.L.Spears, and M.J. Manfra G.W.Charache *AIP. Conf. Proc.* 401, 75 (1997).

[4] C.A.Wang, D.A. Shiau, D.Donetsky, S. Anikeev, G. Belenky and S. Lyuri *Appl. Phys. Lett.* 86 ,101910 (2005).

[5] J.G. Cederberg, M.J. Hafich, R.M. Biefeld and M.N. Palmisiano *J.Cryst.Growth.* 248, 289 (2003).

[6] M.G. Mauk , Z.A. Shellenbarger, J.A. Cox , O.V. Sulima, A.W. Bett , R.L.Mueller , P.E. Sims , J.B. McNeely and L.C. DiNetta *J. Cryst. Growth.* 211**,** 189 (2000).

[7] G.M. Peake , R.J. Shul , C.I.H. Ashby , J.G. Cederberg , M.J.Hafich , R.M. Biefeld and M.N. Palmisiano *J. Vac. Sci. Technol.* B 21, 843 (2003).

[8] M.N. Palmisiano , R.M. Biefeld , J.G. Cederberg , M.J.Hafich and G.M.Peake *AIP. Conf. Proc.* 653, 305 (2003).

[9] O.V. Sulima, K.Swaminathan, T.F. Refaat, N.N. Faleev, A.N.Semenov, V.A.Solov'eV, S.V. Ivanov, M.N. Abedin, U.N. Singh and D. Prather *Electron. Lett.* 42, 55 (2006).

[10] O.V. Sulima, M.G. Mauk , Z.A. Shellenbarger , J.A. Cox , J.V. Li, P.E. Sims , S. Datta S.B. Rafol *IEE. Proc. Optoelectronics 151,* 1 (2004).

[11] H.K. Choi, C.A.Wang , G.W. Turner , M.J. Manfra , D.L. Spears, G.W. Charache, L.R. Danielson and D.M. Depoy *Appl. Phys. Lett.* 71, 3758 (1997).

[12] Z.A. Shellenbarger, G.C. Taylor, R.U. Martinelli and J.M. Carpinelli *AIP. Conf. Proc.* 738, 345 (2004).

[13] D.Donetsky, F. Newman and M. Dashiell Submitted to J. Appl. Phys.

[14] T.S. Moss, G.J. Burrell and B. Ellis *Semiconductor Optoelectronics* (New York: Wiley) 1973.

[15] T.H. Gfroerer, L.P. Priestley, M.F. Fairley and M.W. Wanlass J. *Appl. Phys.* 94,1738 (2003).

[16] L.A.Coldren and S.W. Corzine Diode *Lasers and Integrated Photonic Circuits* (New York: Wiley) 1995.

[17] R.J. Kumar, R.J.Gutmann, J.M. Borrego, P.S.Dutta, C.A.Wang, R.U. Martinelli and G. Nicolls *J. Elec.Mater,* 33, 2, (2004).

FIGURES

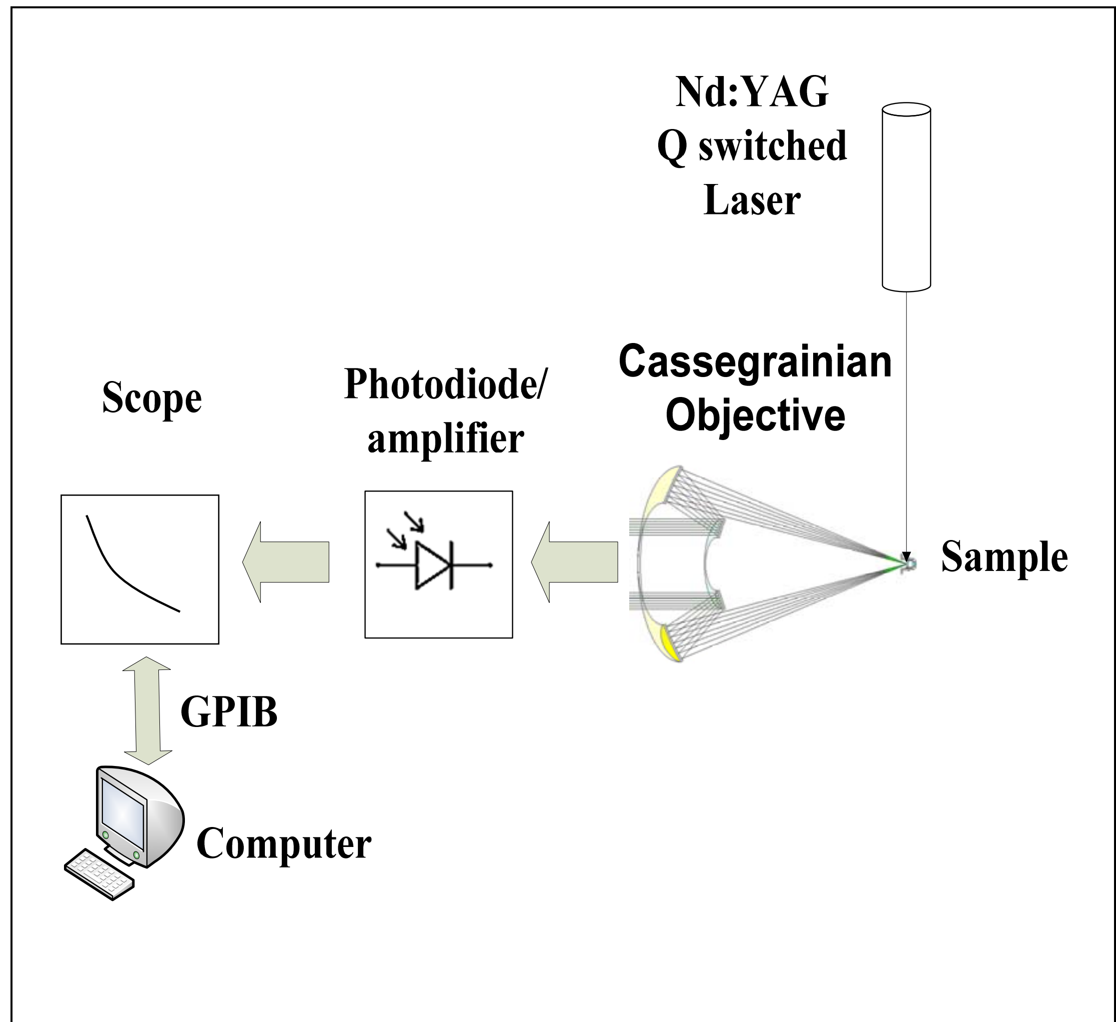

Figure 1.1: Experimental set up used in TRPL technique.

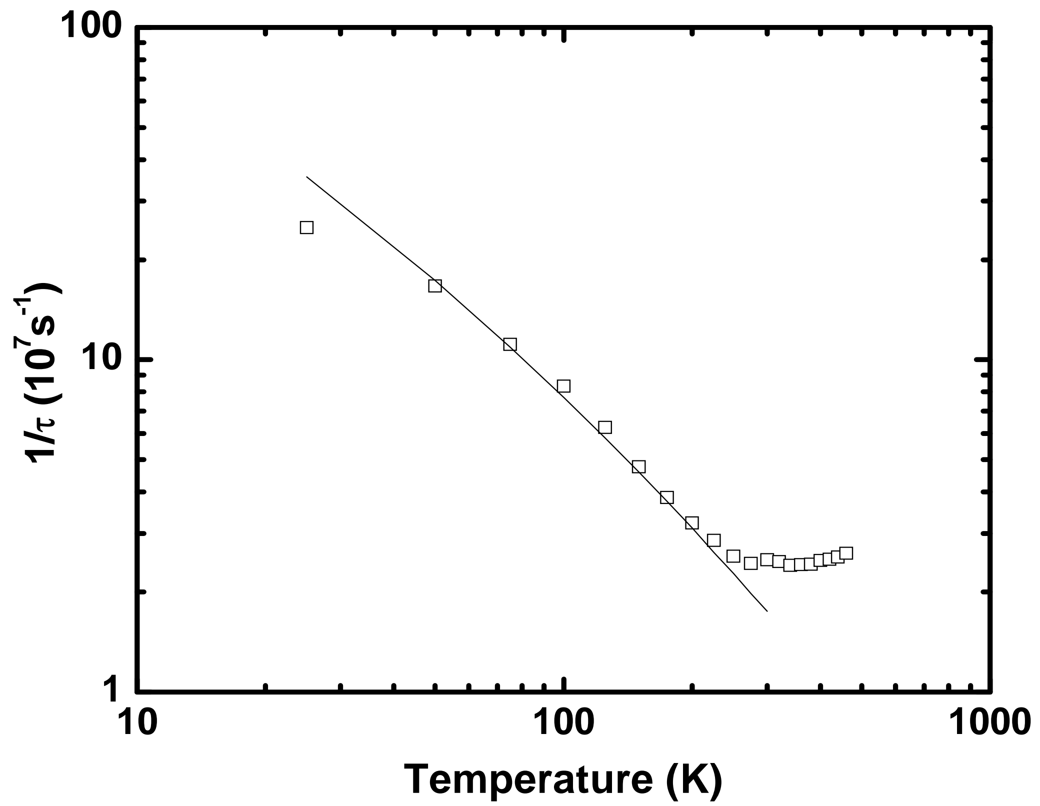

Figure 1.2: Temperature dependence of carrier lifetime of InGaAsSb DH's. Solid dots are experimental points of sample with doping 4×10^{17}; the straight line is a theoretical fit.

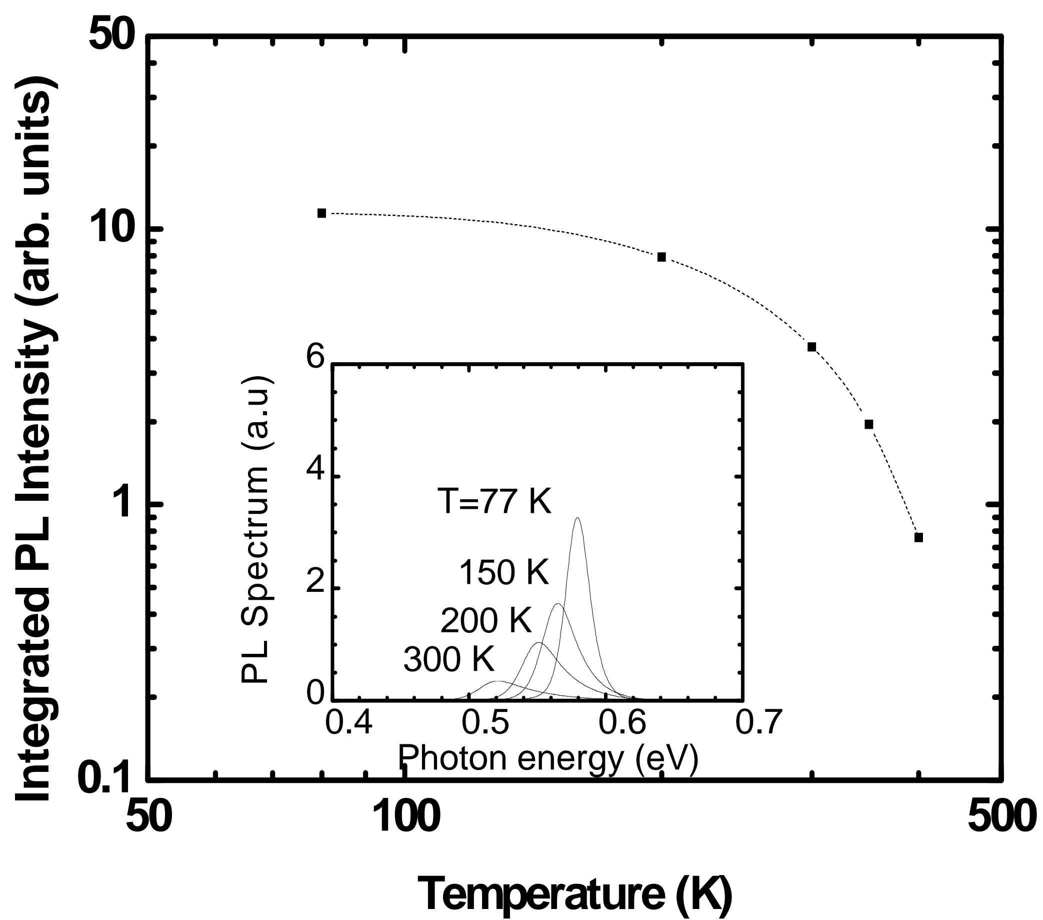

Figure 1.3: Temperature dependence of Integrated PL intensity. Inset shows emission spectra at various temperatures.

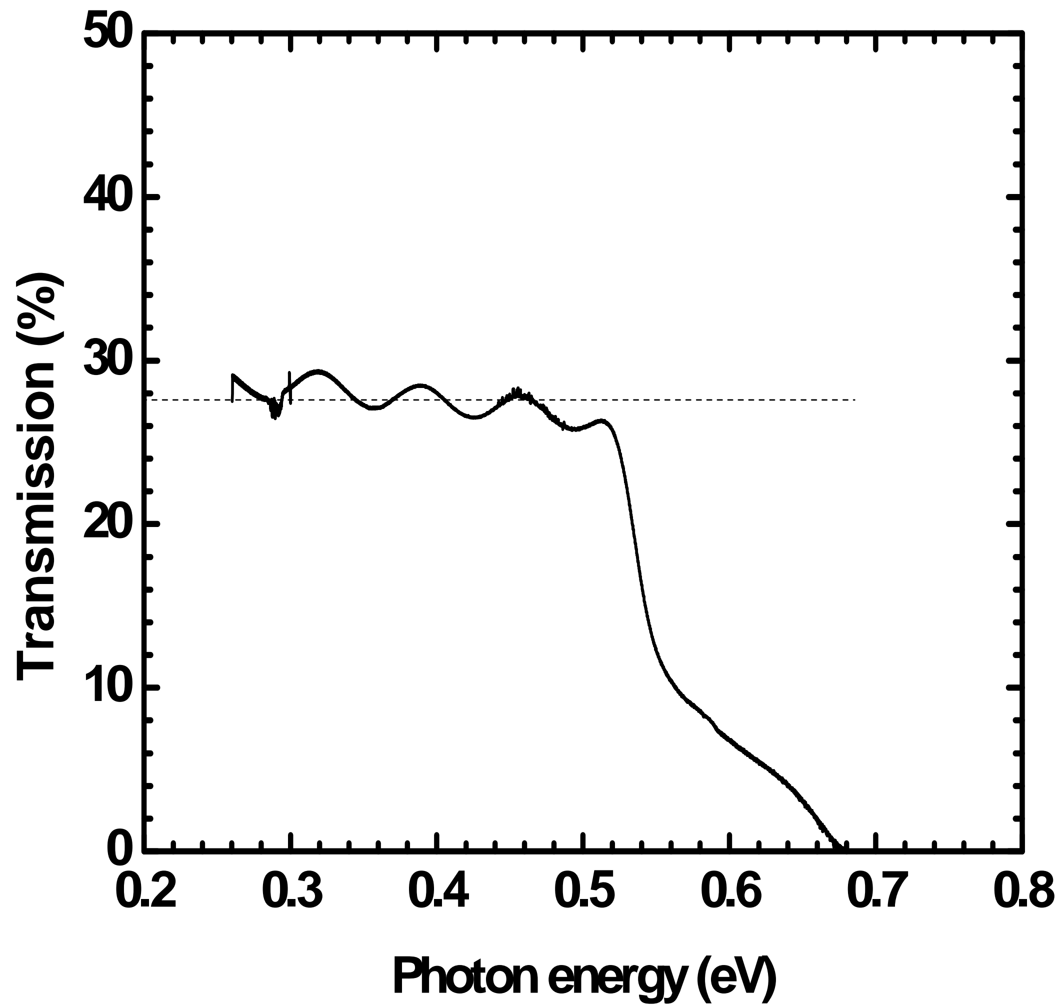

Figure 1.4: Transmission spectrum of 04-959. The dashed line represents the transparency point T/T_0. It is observed that T/T_0 can not be determined accurately.

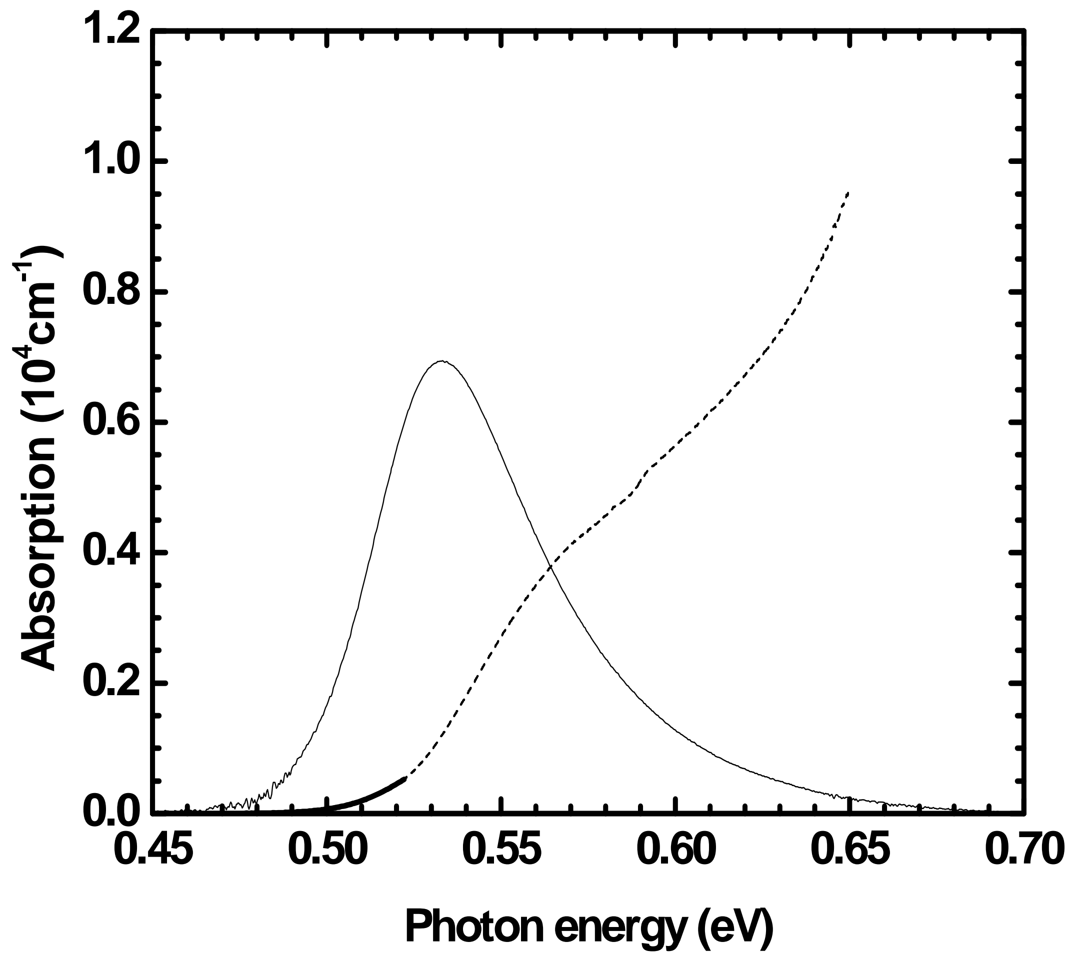

Figure 1.5: Absorption spectrum of heavily doped sample 04-969 (broken line) along with its experimental spontaneous emission spectrum. For energy range till 0.52 eV the experimental PL spectrum was converted to absorption and matched to the experimental spectrum. This is shown as a solid line.

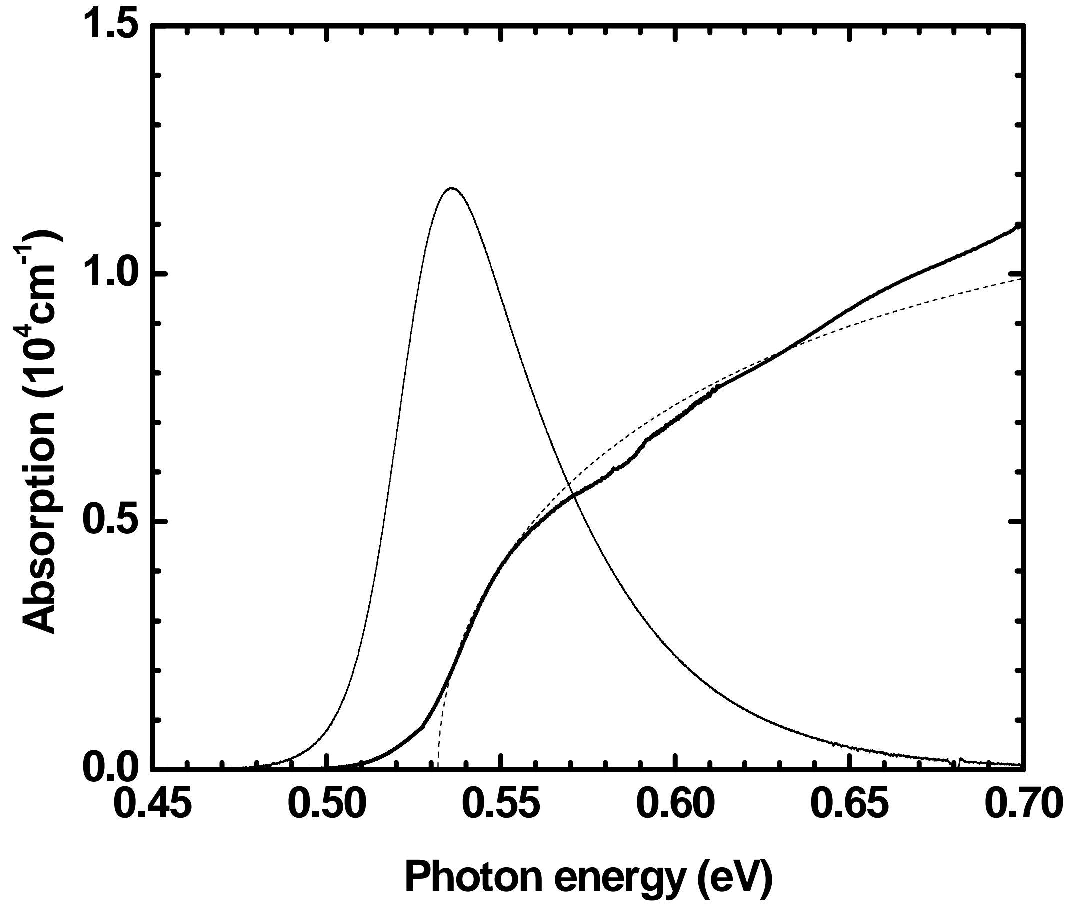

Figure 1.6: Absorption spectrum of moderately doped 04-959 (solid line) and its experimental spontaneous emission spectrum. Square root fit given by the expression: $\frac{A\sqrt{h\nu - E_g}}{h\nu}$ is shown as a broken line.

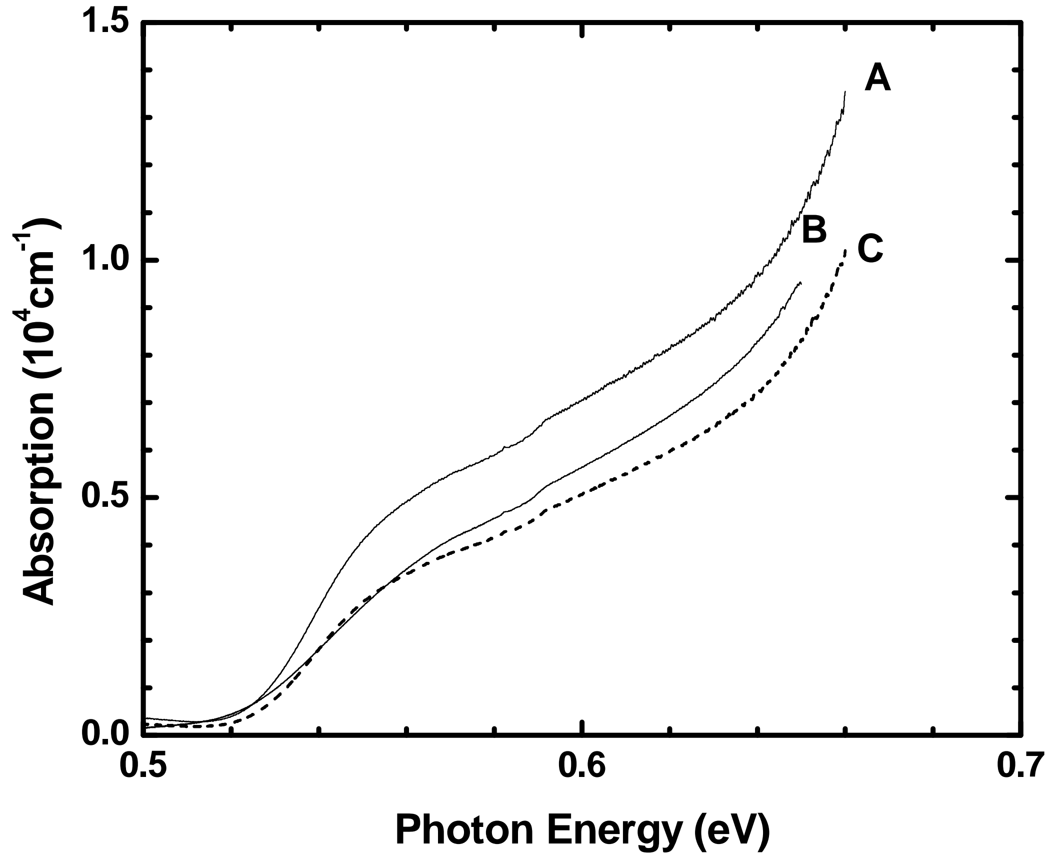

Figure 1.7: Experimental absorption spectrum of 04-959 (A), 04-969 (B) and the calculated spectrum obtained after by BM factor (C). Rapid increase of absorption is seen above 0.65 eV and is attributed to absorption from GaSb substrate. The Luminescence is negligible after this point (see Fig: 4b) and does not affect calculation of Photon Recycling.

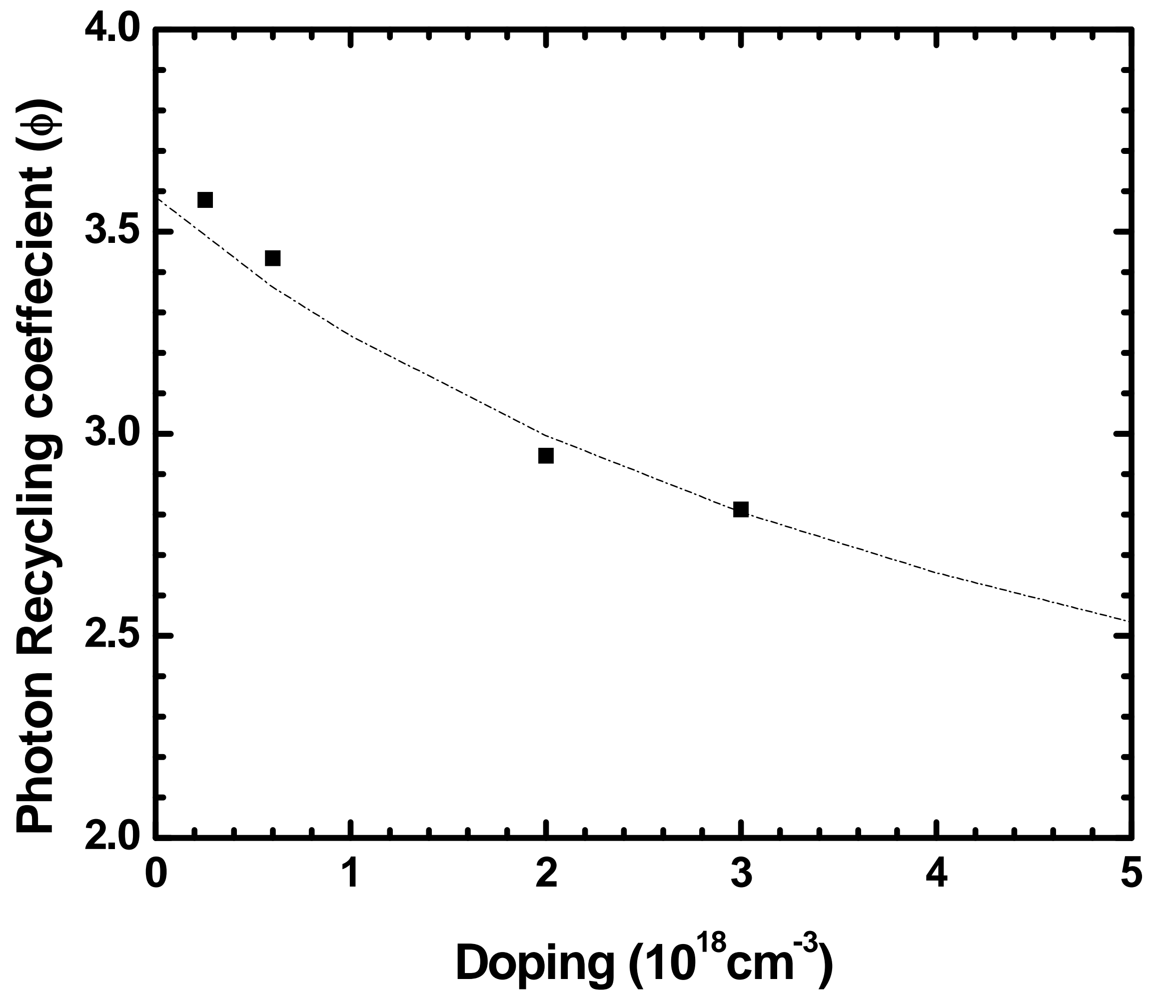

Figure 1.8: PR coefficient obtained from experimental absorption spectrum (points) and from multiplying corresponding BM factors to the absorption spectrum of 04-959(curve).

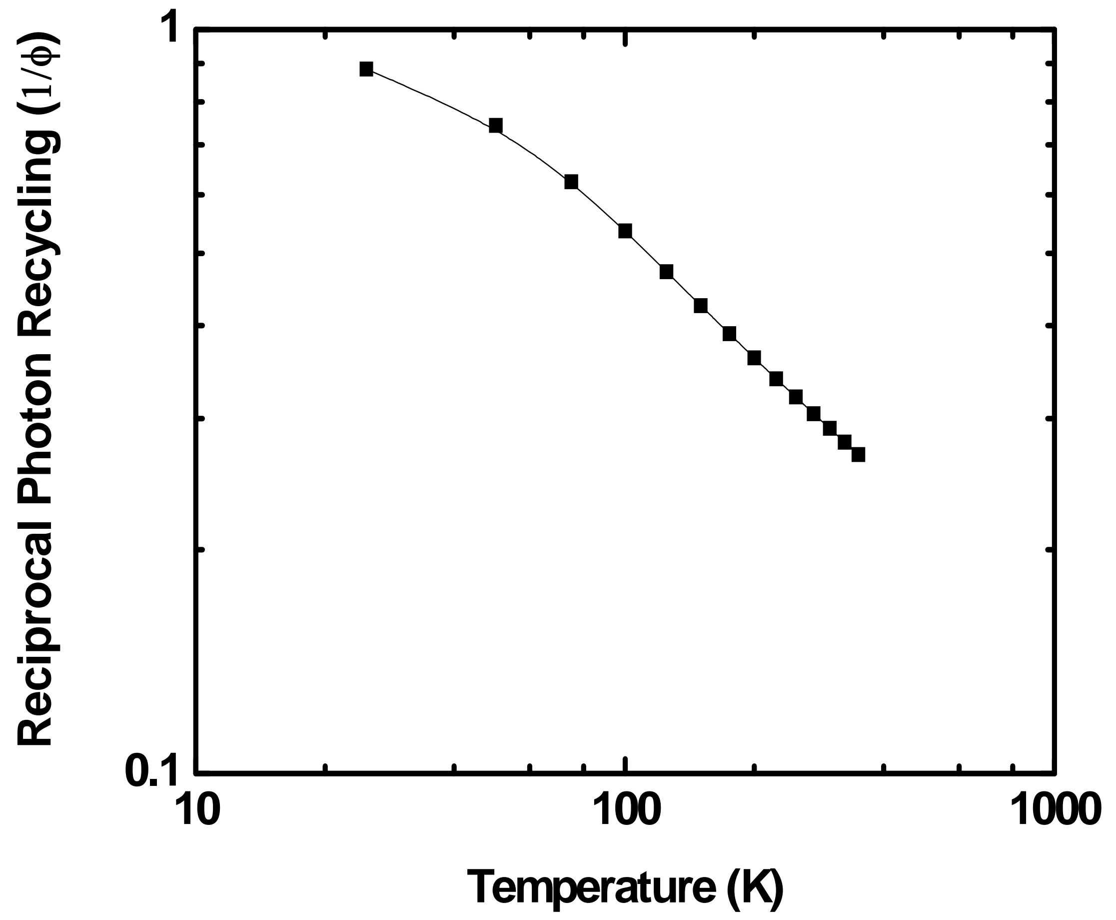

Figure 1.9: Temperature dependence of Photon Recycling for sample doped 4×10^{17}. Photon recycling varies as $T^{0.54.}$

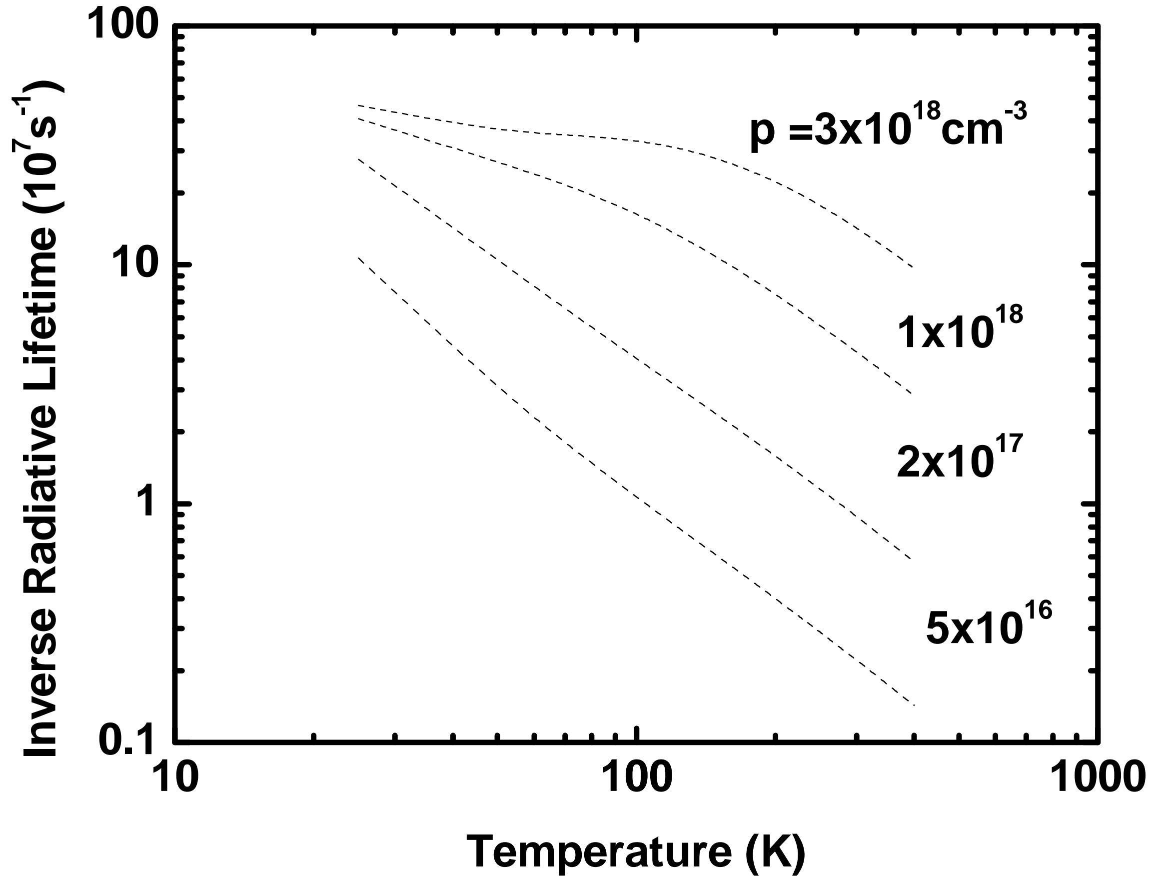

Figure 1.10: Calculated Temperature dependence of Radiative lifetimes of InGaAsSb for various doping concentrations. Temperature dependence of Photon recycling is taken into account.

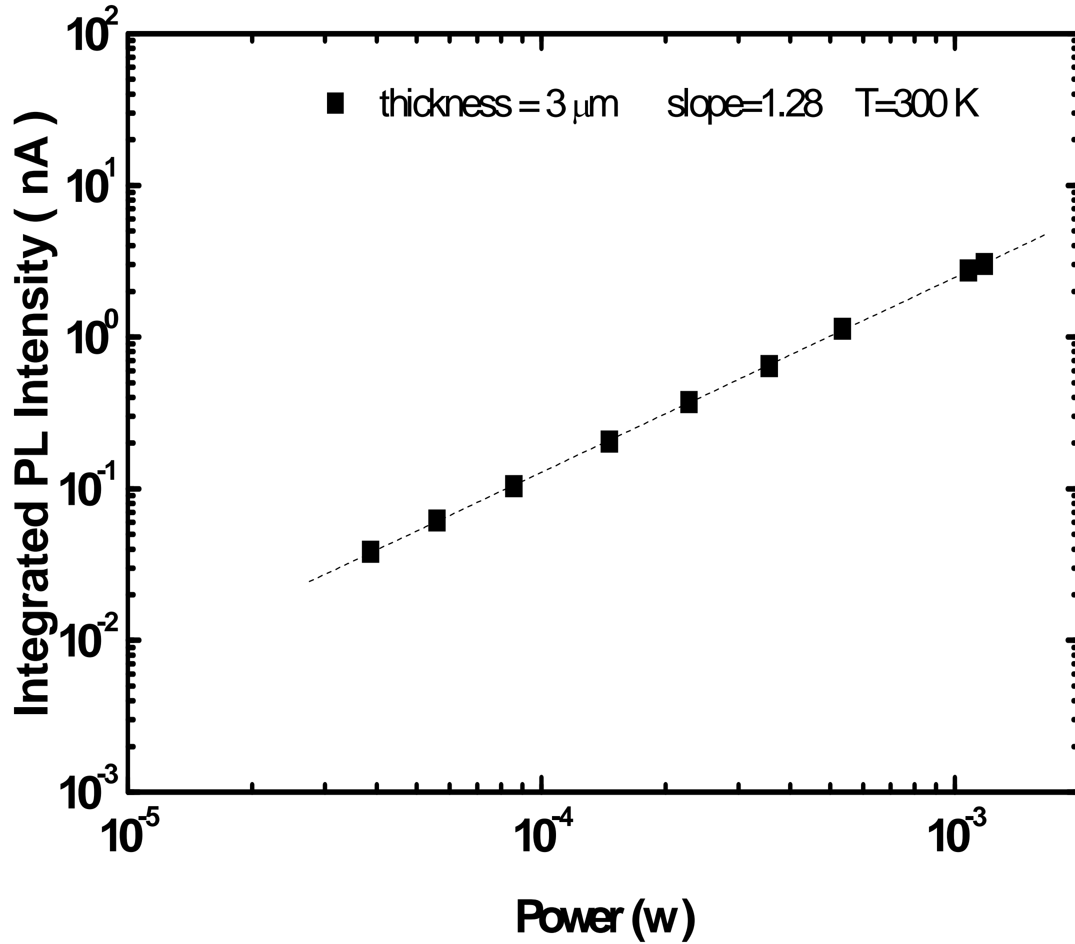

Figure 1.11: Integrated PL intensity as a function of Excess carriers at low excitation. The undoped sample was excited using a 650 nm, 20 mW CW laser, in order to achieve low level of excess carrier concentration. Super linear behavior confirms Shockley Read Hall recombination.

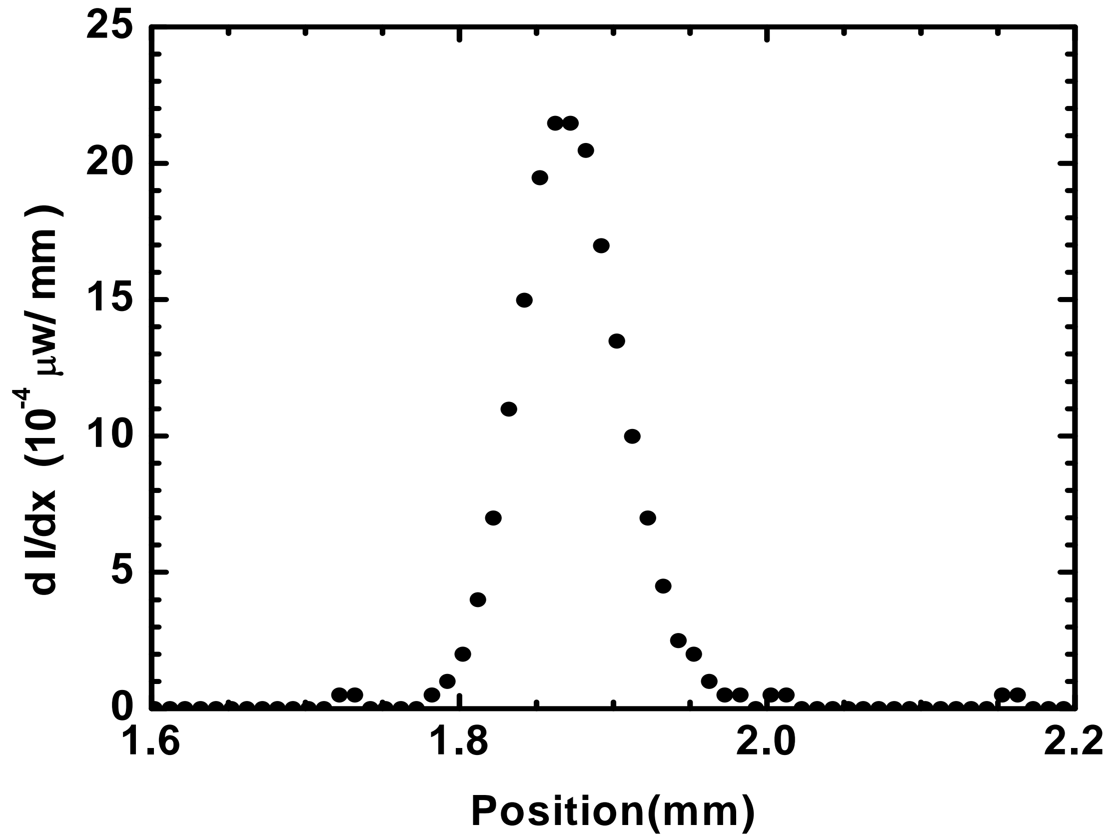

Figure 1.12: Gaussian Profile of the Nd: YAG Laser. The full width half maximum of the profile is taken to be the diameter of the spot.

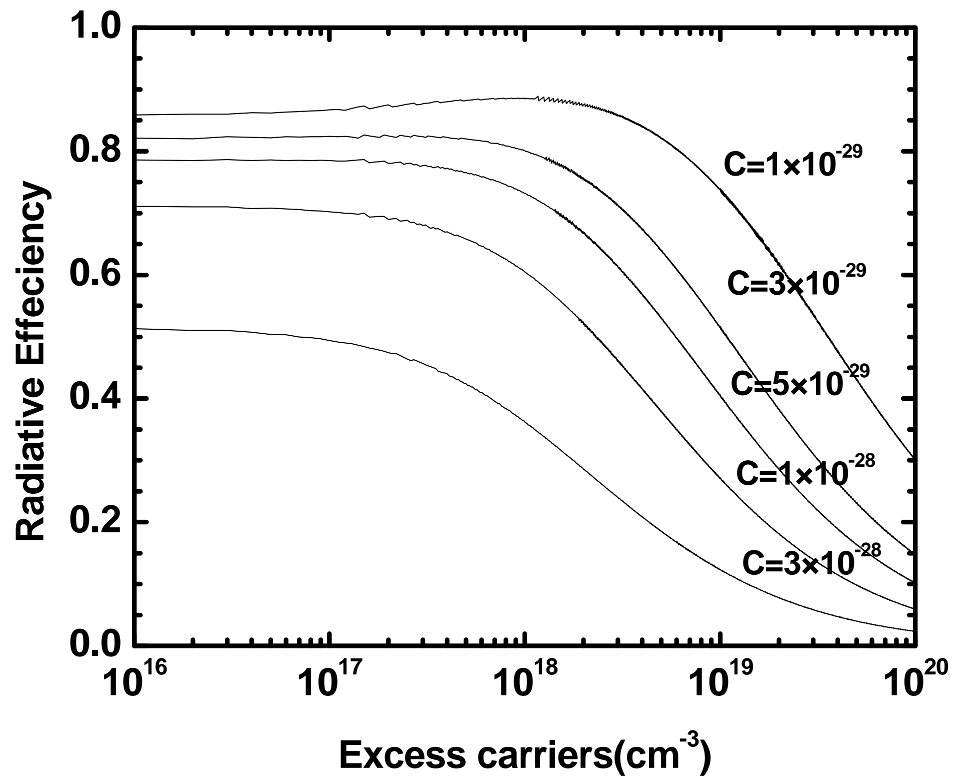

Figure1.13: Radiative efficiency as a function of excess carriers with C as a parameter. Values of A and B were obtained from experimental lifetimes

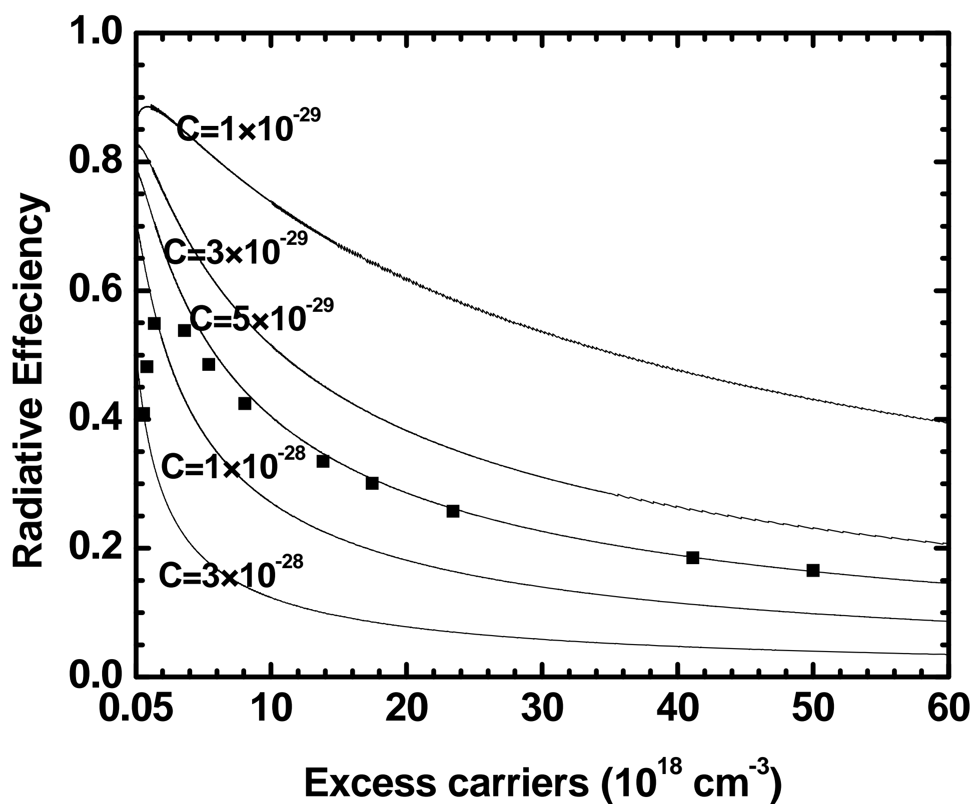

Figure 1.14: Experimental PL per excess carrier concentration of undoped sample, shown as solid points are compared to the simulated radiative efficiency for various values of C. The sample was excited with a 532 nm Q switched Nd: YAG laser with pulse 0.5 ns pulse width and repetition rate of 7 KHz.

Section 2-Surface Passivation of GaSb-based Semiconductor Devices

Introduction

GaSb based systems are promising candidates for optoelectronic devices in the 2-5 μm wavelength range. However antimonides have a high density of defect states at the metal and semiconductor interface that lead to large surface currents[1-2]. It is suggested that oxidation of GaSb at room temperature results in high concentration of elemental antimony at the oxide- GaSb interface leading to increase of the surface leakage current [3]. The presence of elemental antimony leads to the generation of surface states, reducing the minority carrier lifetime and limiting device performance. Passivation of the surface then becomes essential to improve the surface properties of GaSb. Surface passivation using sulfur-based solutions are widely employed as they improve the surface electronic properties[4-7]. Parameters such as barrier height, leakage current, resistivity, breakdown voltage, fixed charges, ageing, and thermal stability are improved by passivation. These improvements are expected to be the result of formation of surface layer consisting of thermally stable S–III and S–V bonds[8]. Though suitable passivation schemes using sulfur based species have been demonstrated, the passivated surface degrades after exposure to the atmosphere with time. Suitable capping is necessary for the passivated surfaces to retain the advantages of passivation[9.]

This investigation focused on achieving passivation by two approaches-creating mesas by micromachining and pulsed anodization technique. Fabrication methods such as Reactive-Ion Etching (RIE) are found to cause damage to the device surface[10-11]. Micromachining by removal of materials with ultrafast (femto-second scale) laser pulses is known to be free from thermal effects and associated damage. Mesas of Schottky interfaces were fabricated by micromachining and their surface currents were compared to untreated Schottky diodes obtained from conventional processing techniques. It was

found that micromachining does not damage the surface as opposed to RIE and that it reduces the surface current in devices when compared to unpassivated devices obtained from lithography.

The other approach employed pulsed anodization technique to passivate the surface of Schottky barriers. This method was proposed as a replacement to standard dielectric films such as silicon oxide and nitrides in order to achieve current confinement in laser diodes[12]. Though natural oxidation of GaSb forms a thin layer of oxide and leads to deleterious effects, pulsed anodization results in the growth of a thick layer of oxide which can be used for passivation. We employed this method to passivate Schottky diodes and achieved a reduction of the device surface current by an order of magnitude. Li et.al[1] obtained 3.6 times reduction in dark current and a further reduction of 9.2 times reduction when a polyimide encapsulation was used. We report 10-11 times reduction of surface current without encapsulating the mesa sidewalls.

A number of metals including Au, Ag, Al, Ni, Cr, In and Pd have been used to fabricate metal-semiconductor interfaces to GaSb[13-14]. Titanium is commonly used in creating ohmic contacts and is known to have good adhesive properties. We decided to utilize the adhesive property of Titanium to fabricate a Ti-GaSb interface as a Schottky barrier. Work on Ti-GaSb Schottky interfaces has not been reported widely in literature. Ideally the barrier height is determined by the difference between the metal work function and electron affinity of the semiconductor. Titanium has a work function of 4.33 eV and GaSb has electron affinity of 4.03 eV[15]. In an ideal case the barrier height of the interface would be 0.3 eV although doubts exist on the exact barrier height and the mechanism of barrier formation[16]. Titanium, when used in ohmic contacts has to be annealed. However without annealing, a rectifying contact is obtained.

Fabrication and characterization of Ti-GaSb Schottky contact

Three types of Au/Ti/GaSb-based Schottky diodes with various diameters of the active area were fabricated and tested: (1) devices with the active area defined by micromachining; (2) devices with the active area defined by photolithography and no surface passivation; (3) devices with the active area defined by the lithography and surface passivation with a native oxide obtained by pulsed anodization method.

A 500 μm thick GaSb substrate was first mechanically polished with 5 μm Aluminum Oxide powder to bring down its thickness to 200 μm. This was followed by lapping using 50 nm TiC powder. The polished substrate was then dipped in dilute HCl solution to remove any oxide from the surface. Then, a low-resistance Ohmic contact was fabricated onto n-side of GaSb by deposition of Ni-Ge-Au-Ni-Au followed by annealing in an inert atmosphere at 250ºC for 2 minutes. A low contact resistance was essential for consistent determination of the diode saturation current. The actual Schottky barriers were formed on another side of the n-GaSb wafer by depositing 5 nm of Ti followed by 100 nm of Au.

Mesas, defined by micromachining, were obtained by forming closed circular grooves by material evaporation with a Spitfire Pro amplified femtosecond laser system from Spectra-Physics. The laser system has a Ti: Sapphire amplifier with a pulse width of 35 femtoseconds and a repetition rate of 1 kHz. A motorized X-Y travel system was programmed to provide circular motion of the samples to create grooves in the sample. A schematic of the set up is shown in Figure 2.1.

It is known that the micromachining process has a threshold power. In fact, no marks on the surface were obtained for average power levels below 10 mW (a 1 kHz repetition rate). Micromachining was carried out at various average power levels: 12, 16, 20, 30 and 40 mW. Grooves with a typical width of several tens of microns were formed. Figure 2.2 shows the groove depth as a function of the power level. The inset shows a schematic of the cross section of the mesa obtained by micromachining. It might be possible to obtain mesas at power levels lower than 10mw by either increasing the repetition rate of the laser or decreasing the velocity of the travel system and it is a subject of further study.

Schottky metal contacts using photolithography were obtained by a metal lift-off method of epi-ready GaSb wafers covered by a photoresist with open windows. The GaSb surface inside the windows was etched in diluted HCL:DI water (1:10) immediately before the metal deposition.

Fabrication steps for the GaSb Schottky diodes with the surface passivated by pulsed anodization are illustrated in Figure 2.3. The process of pulsed anodization for growth of native oxide on a GaSb surface (step 1) has been described in detail in Ref. 11. In step 2 the windows in the oxide were open by oxide removal in diluted HCL using a mask formed by standard photolithography. Later on, Ti/Au layers as described above were deposited (step 3) and lifted-off with the photoresist mask. Finally, the Schottky junctions with depletion regions protected by a native oxide were obtained (step 4).

The devices were soldered onto copper plates in order to carry out measurements of the I-V characteristics. Figure 2.4 shows the IV curves obtained by 4 terminal method in a linear scale depicting the rectifying properties of the Schottky diode. The I-V curves for samples with different diameters are shown in a semi-log scale in Figure 2.5. The diode saturation current I_{sat} was obtained by extrapolation of exponential parts of the I-V characteristics to intersection with Y-axis. Deviation from the exponential dependence at very low currents is due to some offset current.

Results and discussion

Analysis of the obtained data was performed assuming both constant surface current density per unit length J_{surf} (A/m) and constant bulk current density per unit area J_b (A/m^2) as described by the following expression

$$I_{sat} = J_{surf} \cdot 2\pi R + J_b \cdot \pi R^2 \qquad (1)$$

where R is the radius of the mesa. For the mesas obtained by micromachining, the surface current density per unit length (A/m) was obtained as the offset of the dependence of the saturation current per mesa circumference versus radius (Figure 2.6). All experimental points are plotted in Figure 2.6 and lines are drawn through them to determine offsets. Table 1 gives the surface current densities obtained along with the errors in determining them. It is seen that the current densities of mesas obtained by micromachining is lower than that of unpassivated devices obtained by lithography, which has an offset of (11.8 ± 0.16) nA/µm as shown in Figure 2.6. The surface current densities were lowered by 1.64 times for 16 mW, 1.84 times for 20 mW and 2.36 times for 40 mW. These figures were obtained when the maximum error in determining the offsets (Table 1) were added to the actual offsets and compared to the offset of the mesas of unpassivated devices obtained from lithography. This lowering of surface current is seen in mesas obtained by all power levels except 30 mW where a single mesa with a radius of 177 µm causes the offset to be higher than the mesas obtained with other power levels.

The data on saturation current for Schottky diodes with no passivation and for devices with the depletion region surface passivated with a native oxide are presented in Figure 2.7. The saturation currents for the standard devices (solid symbols) have clearly larger values and large data scattering (lower reproducibility) compared to devices with native oxide surface passivation (open symbols). The surface current densities for the standard devices and devices with surface passivation were determined to be (1.18 ±

0.16) nA/μm and (0.11 ± 0.077) nA/μm respectively. The slopes of the linear fits are slightly different and this is attributed to the difference in doping of GaSb substrates.

Thus, the passivation with a native oxide resulted in 10-11 times reduction of the surface current density per unit length which is a considerable improvement.

Conclusion

It was found that machining does not degrade the GaSb surface quality resulting in the surface current densities for Schottky diodes similar or even smaller than those obtained for devices with the unprocessed surface. The observed surface passivation by micromachining can be attributed to formation of a protecting oxide, subject of further study.

Passivation of the surface of GaSb-based Schottky diodes by a native oxide obtained by pulsed anodization was studied. A reduction of the surface current density by 10-11 times has been achieved.

References

[1] J. Li, S. Chuang, O. Sulima and J. Cox, *J.Appl.Phys.* 97, 104506 (2005).

[2] Z.Y. Liu, D.A. Saulys and T.F. Kuech, *Appl.Phys.Lett.* 85, 4391 (2004).

[3] G.P. Schwartz, G.J. Gualtieri, J.E. Griffiths, C.D. Thurmond and B. Schwartz, *J.Electrochem.Soc.* 127, 2488 (1980).

[4] J. Li, S.L Chuang and E. Aifer, *Appl. Phys. Lett.* 85, 4391 (2004).

[5] V.N. Bessolov and M.V. Lebedev, *Semiconductors.* 32, 141 (1998).

[6] Z.Y. Liu, D.A. Saulys, and T.F. Kuech, *Appl.Phys.Lett*. 83, 2587 (2003).

[7] J.A. Robinson and S.E. Mohney, *J.Appl. Phys.* 96, 2684 (2004).

[8] G. Eftekhari, *Vacuum,* 67, 81 (2002).

[9] A. Chavan, A. Chandola and S. Sridaran*, J.Appl.Phys.* 100, 064512 (2006).

[10] C.B. Brooks, M.J. Buie and K.J. Vaidya, *J.Vac.Sci.Technol. A.* 16, 260 (1998).

[11] S.H. Yanga and P.R. Bandaru, *Mat.Sci.Eng.B-Solid.* 143, 27 (2007).

[12] J. Yoon, P. Zory, and R. Menna, *Electrochem.Solid.ST*. 4, C55 (2001).

[13] S.A. Walters and R.H. Williams, *J.Vac.Sci.Technol. B.* 6,1421 (1988).

[14] A.Y. Polyakov, M. Stam and A.G. Milnes, *Mat. Sci.Eng. B-Solid.* 12,337 (1992).

[15] K. Ikossi, M. Goldenberg and J. Mittereder, *Solid.State.Electron.* 46, 1627 (2002).

[16] J. Tersoff, *Phys.Rev.B.* 32, 6968 (1985).

Figures

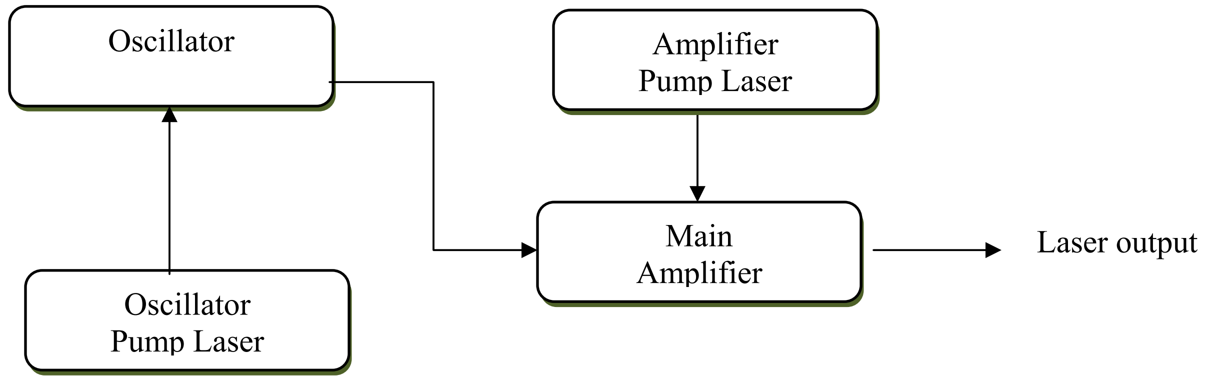

Figure 2.1: Schematic of the micromachining apparatus

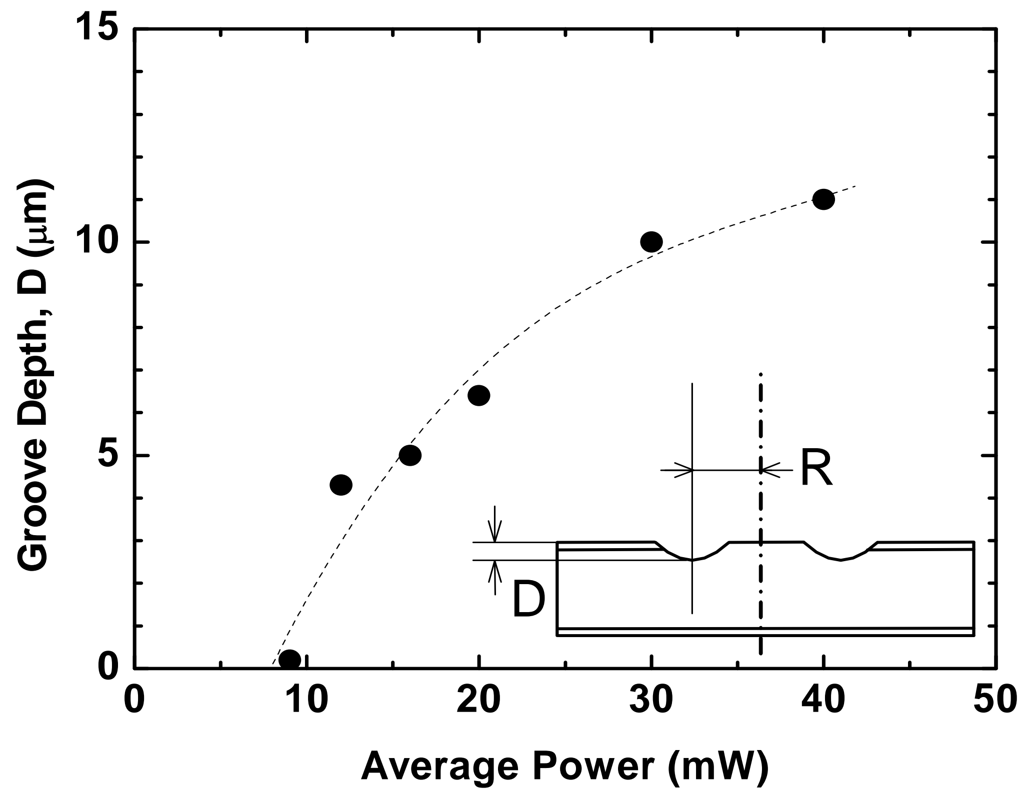

Figure 2.2: Dependence of the groove depth on average laser power. Inset shows the cross section of the sample obtained by micromachining with radius R and depth D.The top contact is a Schottky contact while the bottom contact is ohmic.

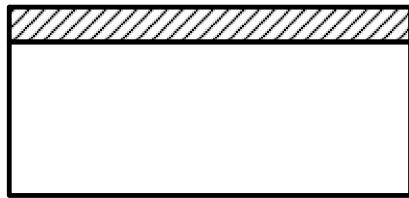

Step 1: Oxide growth

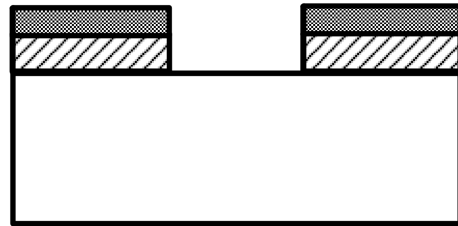

Step 2: Lithography and oxide removal

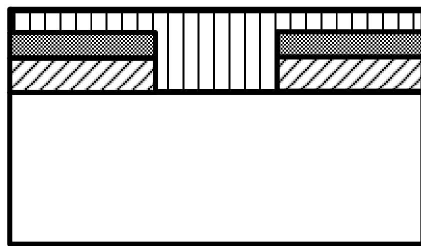

Step 3: Metal deposition

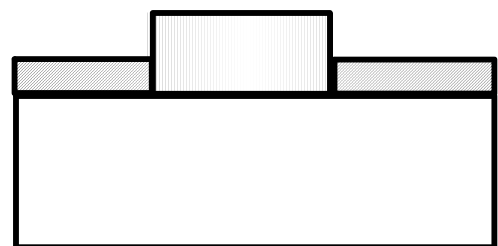

Step 4: Metal liftoff

GaSb substrate Metal Native oxide Photoresist

Figure 2.3: Steps in obtaining the Schottky contact with surface passivation by a native oxide

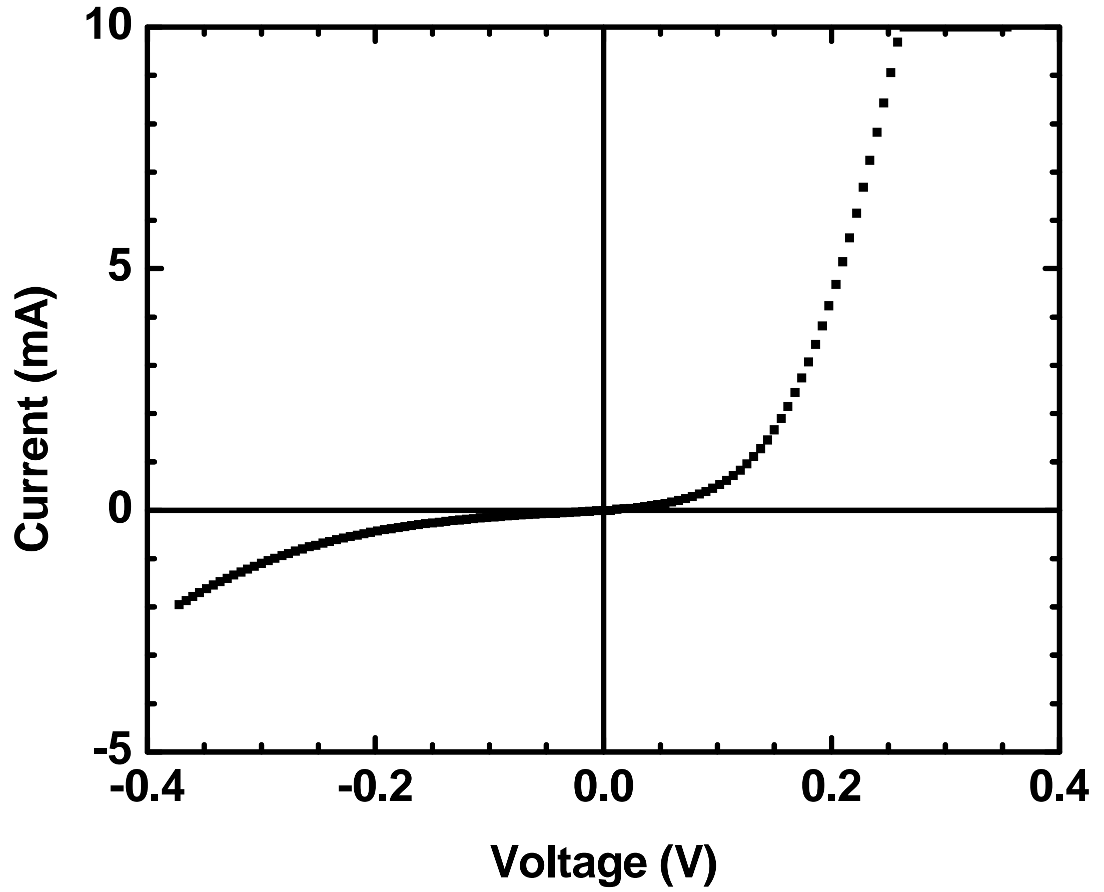

Figure 2.4: I-V characteristics of Schottky diode with mesa radius 236 μm with Ti contact showing the rectifying properties of the barrier

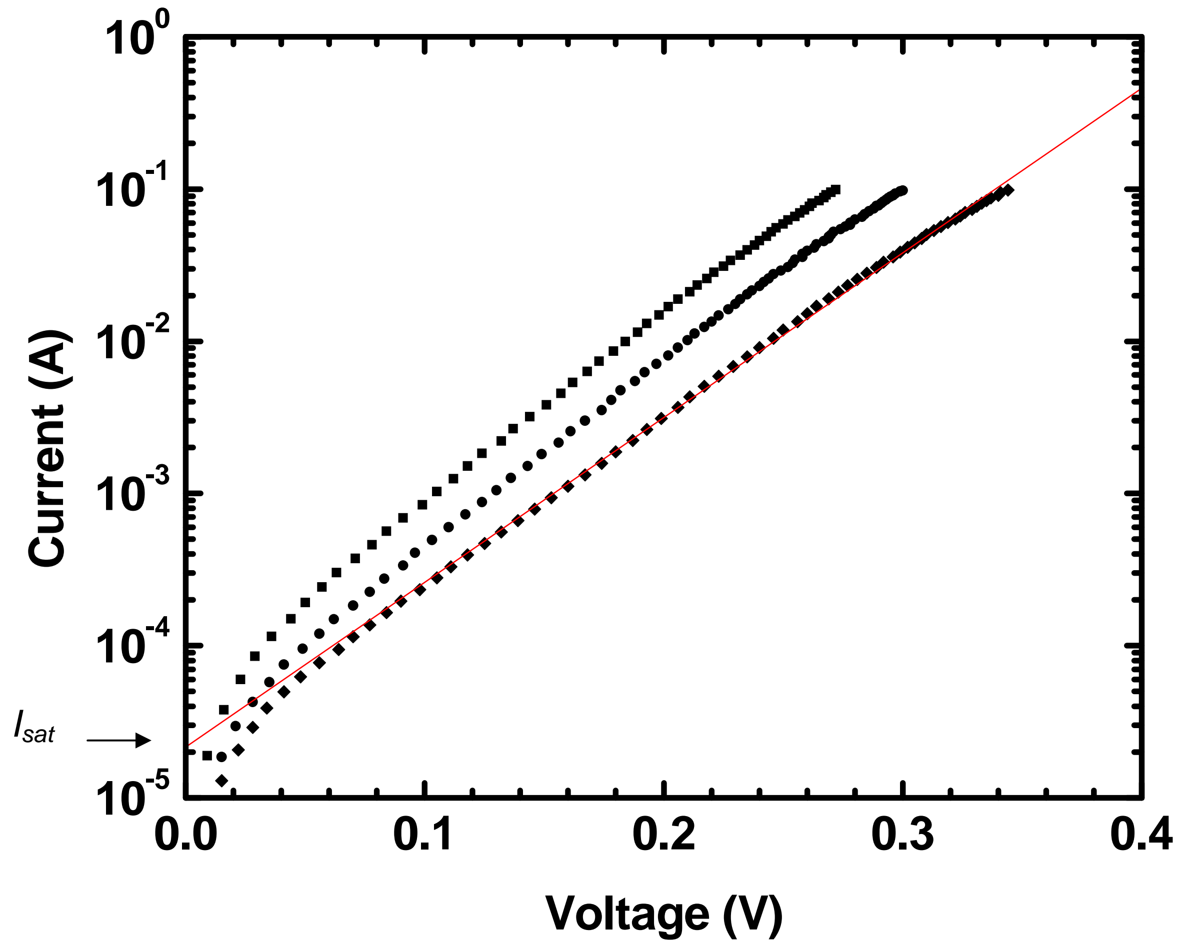

Figure 2.5: I-V characteristics of Schottky diodes with metal contact radii of 65, 120, and 225 μm from bottom to top, respectively.

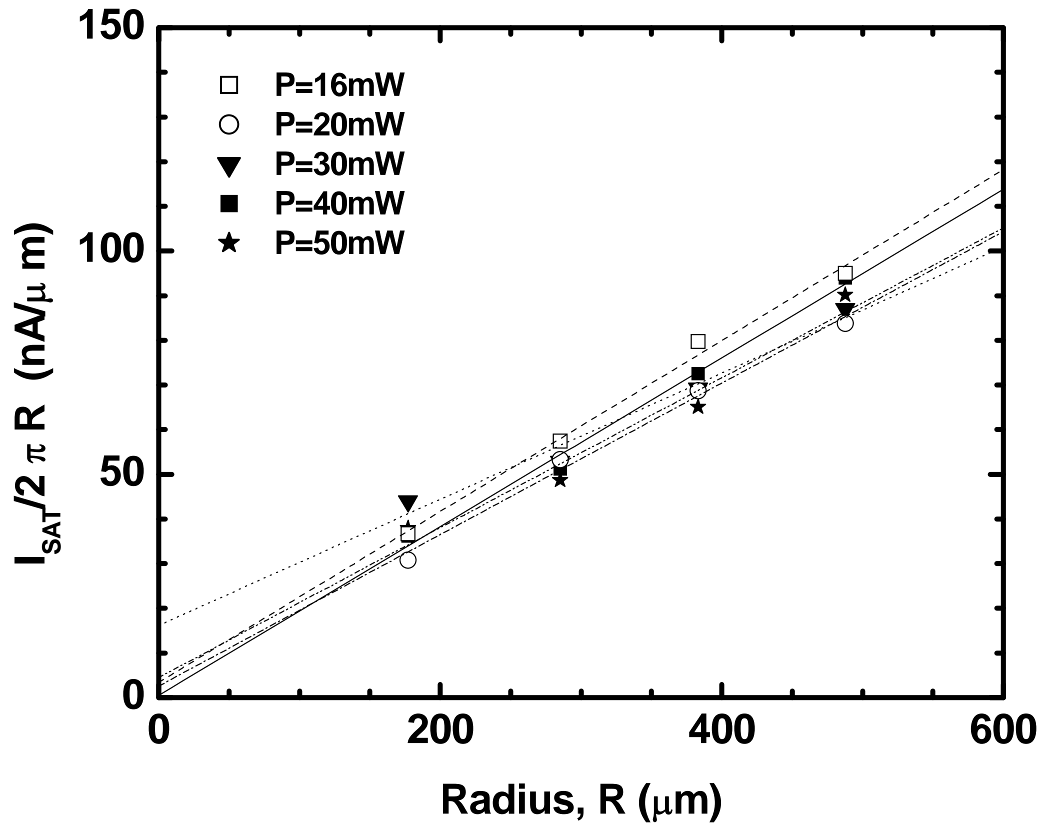

Figure 2.6: Dependence of the saturation current per mesa circumference versus the mesa radius for samples micromachined at different average power levels P.

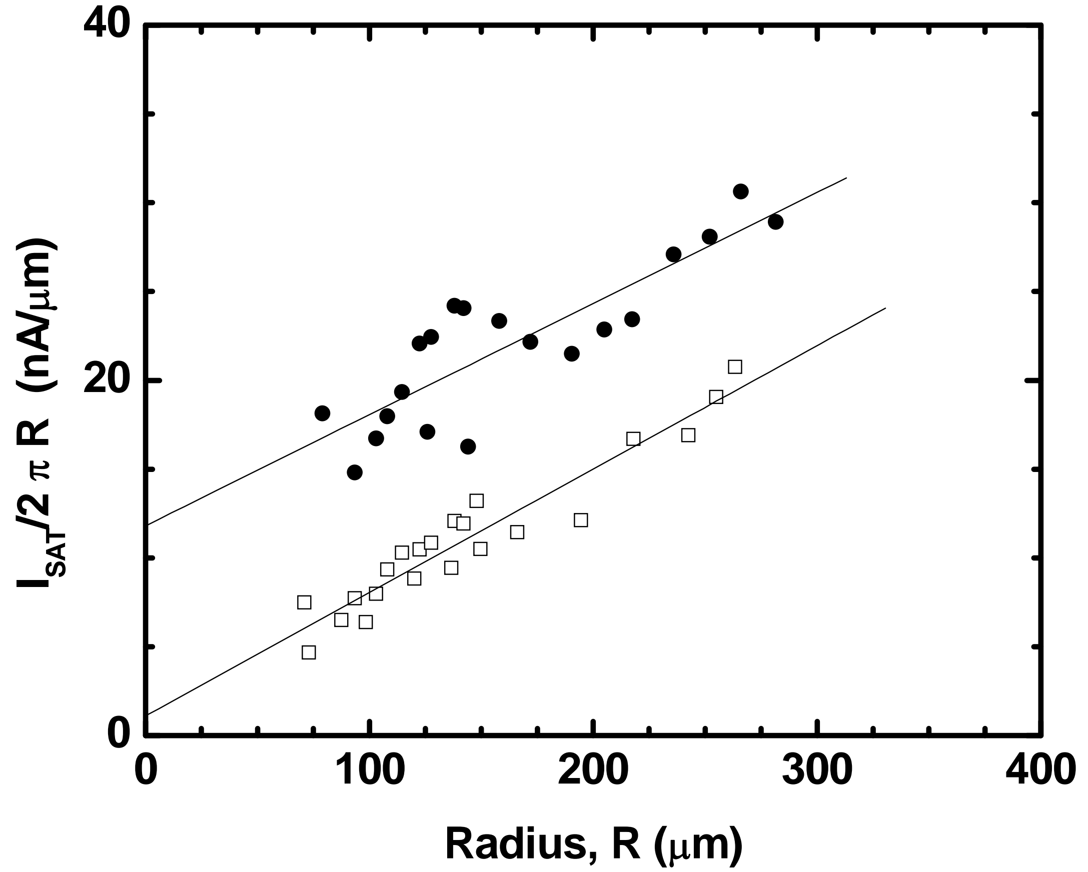

Figure 2.7: The device saturation current per mesa circumference versus the device radius. The circles and squares represent Schottky diodes with no passivation and with oxide passivation. The offsets (which are the surface current densities) were determined to be (1.18 ± 0.16) nA/µm and (0.11 ±0.07) nA/µm, respectively.

Power (mW)	J_{surf} (nA/µm)	Error (nA/µm)
16	**3.4**	**3.8**
20	**2.6**	**3.8**
30	**16.2**	**5.5**
40	**0.5**	**4.5**
50	**4.5**	**8.1**

Table 1: Surface currents obtained for various micromachining power levels and the errors in calculating them